

BIOCHEMISTRY

© Copyright 2004 by the American Chemical Society

Volume 43, Number 49

December 14, 2004

Accelerated Publications

Resolving the Excited State Equilibrium of Peridinin in Solution[†]

Emmanouil Papagiannakis,^{*,‡} Delmar S. Larsen,^{‡,||} Ivo H. M. van Stokkum,[‡] Mikas Vengris,[‡] Roger G. Hiller,[§] and Rienk van Grondelle[‡]

Department of Physics and Astronomy, Faculty of Sciences, Vrije Universiteit, De Boelelaan 1081, 1081 HV, Amsterdam, The Netherlands, and School of Biological Sciences, Macquarie University, New South Wales 2109, Australia

Received September 20, 2004; Revised Manuscript Received October 28, 2004

ABSTRACT: The carotenoid peridinin is abundant in the biosphere, as it is the main pigment bound by the light-harvesting complexes of dinoflagellates, where it collects blue and green sunlight and transfers energy to chlorophyll *a* with high efficiency. Its molecular structure is particularly complex, giving rise to an intricate excited state manifold, which includes a state with charge-transfer character. To disentangle the excited states of peridinin and understand their function in vivo, we applied dispersed pump–probe and pump–dump–probe spectroscopy. The preferential depletion of population from the intramolecular charge transfer state by the dump pulse demonstrates that the S₁ and this charge transfer state are distinct entities. The ensuing dump-induced dynamics illustrates the equilibration of the two states which occurs on the time scale of a few picoseconds. Additionally, the dump pulse populates a short-lived ground state intermediate, which is suggestive of a complex relaxation pathway, probably including structural reorientation or solvation of the ground state. These findings indicate that the unique intramolecular charge transfer state of peridinin is an efficient energy donor to chlorophyll *a* in the peridinin–chlorophyll–protein complex and thus plays a significant role in global light harvesting.

The fixation of atmospheric carbon by oxygenic photosynthetic microorganisms accounts for approximately half of the annual primary production in the biosphere (1). The diverse environmental conditions in the water column (e.g., color and intensity of solar irradiation, temperature, mineral

nutrients) have resulted in a large variety of algal life forms (2), which have developed different light-harvesting strategies in adapting to their environment. The light-harvesting (LH)¹ antennae in the different algae consist of variations on the three transmembrane LHC proteins of plants (2). These variations include a range of different chlorophylls and carotenoids and can be quite similar to those of plants (e.g., the fucoxanthin–chlorophyll–protein, FCP, of chromophytes contains chlorophyll *c*₂ and fucoxanthin in addition to chlorophyll *a*). Besides variations on the LHC proteins, red

[†] This research was supported by The Netherlands Organization for Scientific Research (NWO) via the Dutch Foundation for Earth and Life Sciences (ALW). D.S.L. is grateful to the Human Frontier Science Program Organization for providing financial support with a long-term fellowship. M.V. received financial support from the Stichting voor Fundamenteel Onderzoek der Materie, The Netherlands (FOM).

* Corresponding author. Tel: +31 20 4447934. Fax: +31 20 4447999. E-mail: papagian@nat.vu.nl.

[‡] Vrije Universiteit.

^{||} Current address: Department of Chemistry, University of Southern California, Los Angeles, CA 90089.

[§] Macquarie University.

¹ Abbreviations: LH, light harvesting; PCP, peridinin–chlorophyll–protein; Chl-*a*, chlorophyll *a*; EET, excitation energy transfer; ICT, intramolecular charge transfer; SE, stimulated emission; ESA, excited state absorption; PP, pump–probe; PDP, pump–dump–probe; ΔΔOD, double difference in optical density; SADS, species-associated difference spectrum; GSI, ground state intermediate.

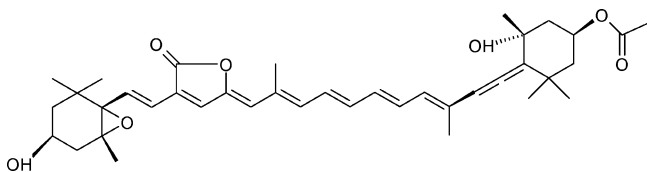


FIGURE 1: Molecular structure of peridinin.

algae and cryptophytes contain phycobiliproteins, and the dinoflagellates contain the water-soluble peridinin–chlorophyll–protein, PCP. These different photosynthetic antennae are adapted to harvest the blue/green light available in aquatic environments, and in some of them the amount of carotenoids exceeds that of chlorophylls.

The light-harvesting protein with the highest observed carotenoid:chlorophyll ratio is the water-soluble PCP complex from dinoflagellates which binds peridinin and chlorophyll *a* (Chl-*a*) molecules in a 4:1 ratio. The crystal structure of PCP from *Amphidinium carterae* (3) shows that in its monomeric unit four peridinin molecules are in van der Waals contact with each other and a Chl-*a* molecule, which they surround. The peridinins in PCP are excellent light harvesters; they have strong absorption from 450 to 550 nm and reach an efficiency of excitation energy transfer (EET) to Chl-*a* of 90% (4), which is achieved by its peculiar excited state manifold (5, 6).

Peridinin is probably the least symmetric carotenoid (7) as its structure contains a conjugated lactone ring, an allene moiety, and two terminal rings (Figure 1). Understanding its function *in vivo* requires the evaluation of its inherent properties in solution, unperturbed by the protein scaffolding or energy transfer to Chl-*a*. Such studies have shown that, in contrast to typical plant or bacterial carotenoids and due to the complex molecular structure of peridinin, the relaxation pathways after excitation to the strongly absorbing $1B_u^+$ state (S_2) depend strongly on the polarity of the environment (8–11). In the nonpolar environment of hexane, the relaxation of S_2 leads to the population of the $2A_g^-$ (S_1) state which has a 160 ps lifetime (8), as expected for a carotenoid with eight conjugated π -electrons. However, in polar solvents, such as methanol and ethylene glycol, markedly different transient absorption and fluorescence spectra were observed, and the excited state lifetime was found to be ~ 10 ps, considerably shorter than in hexane (8, 10). To account for these observations, a model entailing the population and stabilization of an intramolecular charge transfer (ICT) state in polar solvents (9, 11) was proposed, which involved a structural rearrangement (11).

PCP binds its peridinin molecules in a polar protein environment, which also leads to the population of the ICT state after excitation (6). However, the complex excited state manifold of peridinin and the parallel transient absorption dynamics of Chl-*a*, which is rapidly excited via energy transfer, hinder the precise determination of the relaxation scheme. Measurements in a polar solvent such as methanol, where peridinin may be expected to have properties similar to those *in vivo*, become vital for understanding its function in the PCP complex. Thus far, neither experiments nor calculations have generated a consistent picture describing the relation between the S_1 and the ICT state: Are they one state (12) or two separate states (13) or do the ICT characteristics reflect a specific position on the S_1 potential

surface (11)? Furthermore, what are the implications of their relationship for the biological function of peridinin in PCP?

Exploration of complex molecular mechanisms, such as the relaxation dynamics of peridinin, demands novel spectroscopic tools, such as the multipulse transient absorption techniques (14–19). The introduction of a third pulse, resonant with a stimulated emission (SE) band, in the standard pump–probe scheme depletes the emissive state by dumping excited state population to the electronic ground state at specific and controlled times. Probing the effect of the dump pulse on the transient absorption signals in the bleach and excited state absorption (ESA) regions allows for the identification of coexisting excited species with overlapping spectra, as only the contribution of the depleted state will be affected by the dump. The development of a pump–dump–probe experimental setup with broad-band detection, combined with the global analysis of the full data set, enabled us to elucidate complex parallel decay dynamics in β -carotene (18) and in the chromophores of the photoactive yellow protein (19) and the green fluorescent protein (20).

To address the aforementioned question about how the excited states of peridinin are connected and to understand their biological function in PCP, we performed a pump–dump–probe experiment on peridinin in methanol with 530 nm excitation and 800 nm dump. The SE of the ICT state was dumped 3 ps after excitation by the 800 nm pulses, and the resulting dynamics was probed across the visible range.

MATERIALS AND METHODS

Sample Preparation. Peridinin was extracted from *Amphidinium carterae* thylakoids by the method of Martinson and Plumley (21) and was purified by reverse-phase HPLC using an Alltech C18 column. The samples were dried *in vacuo* and stored at -20°C ; they were dissolved in methanol to a peak absorbance (475 nm) of ~ 0.3 in a 1 mm quartz cuvette.

Ultrafast Transient Absorption. The femtosecond dispersed pump–dump–probe apparatus has been described in detail earlier (19). The basis of the system is a 1 kHz amplified Ti:sapphire system delivering 450 μJ , 60 fs, 800 nm pulses. Part of the output of the amplifier pumped a homemade noncollinear optical parametric amplifier (NOPA) tuned at 530 nm, while for dumping we used 800 nm pulses directly from the amplifier. Another fraction of the 800 nm light was focused in a slowly translating CaF_2 crystal to generate the single-filament white light continuum used for broad-band probing. The white light was steered and focused onto the sample by reflective optics, decreasing the group velocity dispersion to typically ~ 300 fs over the range of 400–700 nm. The pump and dump pulses were both set at magic angle (54.7°) compared to the polarization of the probe light. The time and wavelength resolutions of our experiments are 125 fs and 1 nm, respectively, while the average noise level is < 1 mOD.

Data Presentation and Analysis. The measurement of pump–probe signals in the presence (PDP) and in the absence of the dump pulse (PP) allows the definition of a double difference absorption signal

$$\Delta\Delta\text{OD}(\lambda, t, \tau) = \text{PDP}(\lambda, t, \tau) - \text{PP}(\lambda, t) \quad (1)$$

where λ is the probe wavelength, t the probe delay, and τ

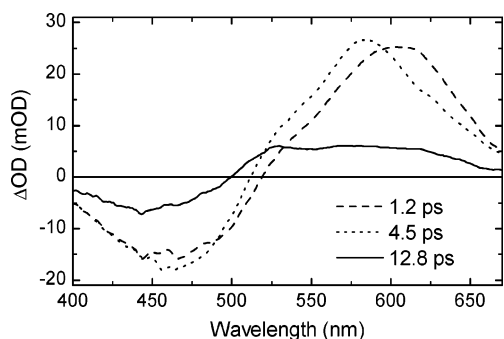


FIGURE 2: SADS and associated lifetimes estimated by applying a sequential decay scheme in global analysis of peridinin in methanol after excitation of the S_2 state at 530 nm.

the dump time with respect to the pump pulse. The $\Delta\Delta\text{OD}$ signal is useful for visualizing the dump-induced effects because it has nonzero amplitude only when the dump pulse induces an effect on the system. The $\Delta\Delta\text{OD}$ signal inherently contains the PP dynamics (and not only a population loss), and to examine whether the dumping induces *additional* dynamics, it is convenient to define the relative double difference signal as

$$\Delta\Delta\text{OD}_{\text{rel}} = \Delta\Delta\text{OD}(\lambda, t, \tau) / \text{PP}(\lambda, t) \quad (2)$$

Global and target analysis was used to fit the collected data (22, 23). First we applied a sequential modeling scheme to fit the PP data, which contains four discrete species that evolve into each other with increasing lifetimes. The data are described by the estimated set of species-associated difference spectra (SADS) and their respective lifetimes. This description of the data is phenomenological, and each SADS does not necessarily represent the spectrum of a *pure* state. Subsequently, to produce a physical model and allow for complex dynamic evolution, we adopted a specific connectivity scheme in the target analysis and simultaneously fitted the PP and PDP data. In this way, each compartment of the model represents a discrete state with a characteristic spectrum and concentration temporal profile.

RESULTS

Peridinin Pump–Probe Dynamics. Peridinin was excited at 530 nm, a wavelength that after the relaxation of the S_2 state leads to enhanced ICT-like features (11), and the transient absorption from 400 to 700 nm was then monitored. The sequential scheme in the global analysis identified four decay components; the resulting SADS and their lifetimes are shown in Figure 2, except for the one depicting the short-lived S_2 state which is distorted by cross-phase modulation. The first SADS (dashed line) describes the excited species that is generated by the sub-100 fs decay of S_2 (11) and has a strong ESA band peaking at 605 nm. Its 1.2 ps lifetime describes the evolution into the second SADS (dotted line) which is similar in shape, albeit slightly narrower and blue shifted, peaking at 585 nm. Notably, the ESA shoulder below 540 nm, the region associated with the S_1 ESA (11), is present in both SADS but is rather weak. The 4.5 ps lifetime of the second SADS describes a significant loss of amplitude and spectral evolution to the third SADS (solid line) which decays to the ground state with a 12.8 ps time constant. In

this SADS the relative amplitude in the region below 540 nm is enhanced, and furthermore, the signal around 500 nm becomes positive. This indicates that the significant loss of ESA around 590 nm which is characterized by the 4.5 ps time constant is accompanied by an increase of ESA around 500 nm.

The pump–probe data and the sequential global analysis confirm the earlier observations (11) that 530 nm excitation of peridinin in methanol results in a dominant ICT character at early times and the presence of a picosecond relaxation component. Our data and the global analysis further illustrate that this relaxation component corresponds to a blue shift of ESA and that the additional decay component on the time scale of a few picoseconds which depends on the excitation wavelength (11) corresponds to a significant spectral change (dots to solid line in Figure 2). Despite the significant spectral information, these results are too ambiguous to allow for definitive conclusions about the connectivity of the S_1 and ICT states. Nonetheless, we do observe that, at later delays, a shoulder below 540 nm, the spectral feature associated with the S_1 state, develops in the PP spectrum. Hence, a mechanism which populates S_1 on the time scale of a few picoseconds is implied; such a process cannot involve the fast-decaying S_2 state but presumably the longer-lived ICT state.

Dumping the ICT State of Peridinin. The PDP and $\Delta\Delta\text{OD}$ (eq 1) kinetic trace signals, measured when a 800 nm dump pulse is placed 3 ps after excitation of peridinin at 530 nm, are contrasted with the corresponding PP traces in Figure 3: 435 nm (bleach), 535 nm (ESA shoulder), and 590 nm (ESA peak). The PDP traces coincide with the PP traces until 3 ps, when the 800 nm pulse interacts with the excited peridinin. The effect of the dump pulse on the transient absorption signals is clearly manifested as a loss of excited state population (decrease of ESA signals) and a concomitant gain of ground state population (decrease of bleach). The lowest panel shows the $\Delta\Delta\text{OD}_{\text{rel}}$ signals at the same three wavelengths (eq 2), where the contribution of the PP decay is stripped from the $\Delta\Delta\text{OD}$ signals and the underlying *additional* dump-induced dynamics is unveiled. At 590 nm the loss is instantaneous (instrument response limited), while at 435 and 535 nm the response is slower with more complex dynamics.

The comparison of the $\Delta\Delta\text{OD}_{\text{rel}}$ traces demonstrates that the dump pulse induces additional dynamics to the system. This dynamics is clearly illustrated in Figure 4, which contrasts the PP time-resolved spectra (solid lines) measured at 3.5, 5, and 14 ps with the corresponding $\Delta\Delta\text{OD}$ spectra which were measured with the dump pulse at 3 ps (dashed lines, inverted and normalized at the peak to allow comparison). The $\Delta\Delta\text{OD}$ spectrum measured at 3.5 ps (0.5 ps after the dump) lacks part of the bleach and the S_1 part of the PP spectrum. This implies that the dump is not populating immediately the equilibrated ground state and that it is selectively depleting a part of the ESA. The comparison of the spectra measured at 5 ps reveals that 2 ps after the dump the difference in the bleach region has disappeared. In sharp contrast, a difference persists in the 525 nm region, showing that the S_1 population is not affected by the dump pulse on this time scale. At 14 ps, 11 ps after the dump, the PP and $\Delta\Delta\text{OD}$ spectra are identical, indicating that at this delay the loss of excited state population is homogeneous.

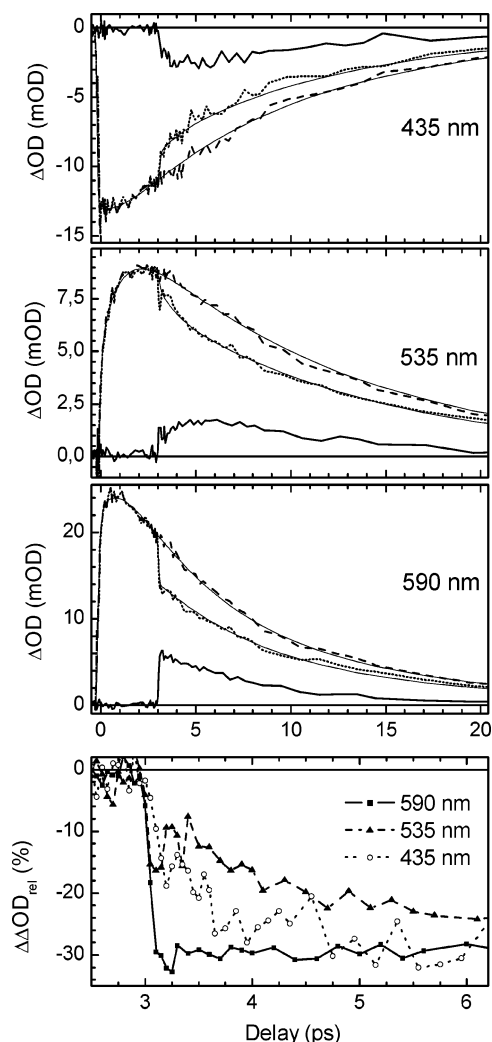


FIGURE 3: Pump-probe (dashed lines) and pump-dump-probe (dotted lines) kinetic traces of peridinin in methanol measured at 435, 535, and 590 nm. The thin solid lines through the data denote the target analysis fit, while the thick solid lines correspond to the depletion ($-\Delta\Delta\text{OD}$) signal. The lowest panel contains the relative loss signals, $\Delta\Delta\text{OD}_{\text{rel}}$, at 435, 535, and 590 nm. Note the different horizontal scale of the lowest panel.

The instantaneous loss of signal at 590 nm indicates that the dump pulse depopulates the ICT state rapidly. If the excited population were dumped directly into the equilibrated ground state, then the response in the bleach region, probed at 435 nm, would also be instantaneous, exhibiting no resolvable recovery dynamics (18). However, the dump-induced recovery at 435 nm is noticeably slower (~ 1 ps, Figures 3 and 4) than the loss at 590 nm, implying that the dumped population proceeds via a ground state intermediate (GSI) before filling the bleach. Similarly, an effect on the S_1 population is only observed at later delays; at 535 nm, where the ESA contains a significant contribution from the S_1 population, the response to the dump is on the time scale of a few picoseconds, and the loss signal keeps growing 4 ps after the dump (Figure 3, lowest panel). This shows that even though the two excited states, S_1 and ICT, have distinct populations, they equilibrate on the time scale of a few picoseconds, as postulated after the analysis of the pump-probe data above.

Modeling the Excited States. The PP and PDP data described above strongly suggest that the S_1 and ICT states

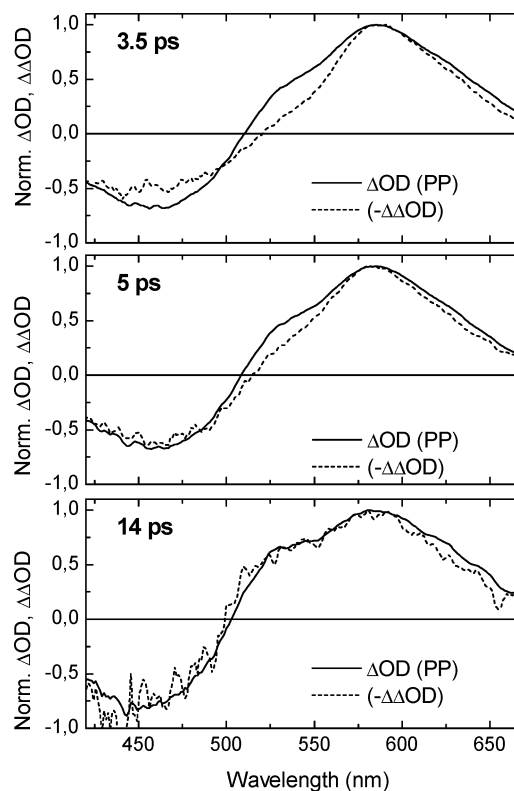


FIGURE 4: Comparison between the pump-probe spectra (solid lines) and the $\Delta\Delta\text{OD}$ spectra (dashed lines) measured at probe delays of 3.5, 5, and 14 ps (dump at 3 ps). All spectra have been normalized at the peak of the excited state absorption, and the $\Delta\Delta\text{OD}$ have been inverted to facilitate the comparison of their shapes. The absolute magnitude of the signals can be seen in Figure 3.

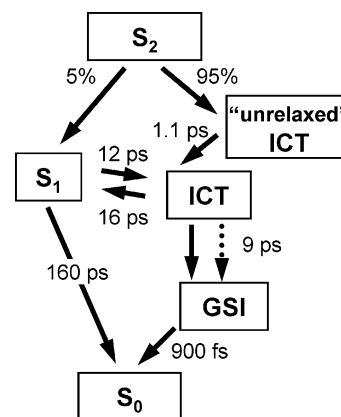


FIGURE 5: Kinetic scheme that has been used to model the excited states of peridinin.

of peridinin are separate, yet coupled entities. To incorporate all of the above findings and describe the reactions underlying the observed signals, we used the connectivity scheme shown in Figure 5 to simultaneously model the PP and PDP experiments with a target analysis. The use of five compartments was essential for obtaining a satisfactory fit. Relaxation from the initially excited S_2 state occurs through two separate (branched) pathways, populating either the S_1 state or the ICT state. Of these, only the latter involves an unrelaxed intermediate similar to other carotenoids (24, 25). Even though the S_1 state might also be undergoing thermal relaxation, it has not been possible to resolve it, because its red wing overlaps with the ICT state and, moreover, the

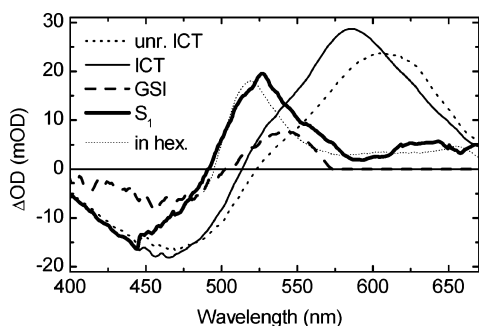


FIGURE 6: SADS and decay lifetimes of the excited states of peridinin as estimated by the target analysis by using the model shown in Figure 5. In addition to the SADS, we also present the pump-probe spectrum measured in hexane (thin dotted line) for comparison with the S_1 SADS (thick solid line).

amount of S_1 produced directly from the higher S_2 state is small after 530 nm excitation (see below). Both the natural and the dumped evolution of the ICT state populates a GSI state, which in turn decays into the equilibrated ground state. In addition to their decay pathways, the populations of the S_1 and ICT states are allowed to equilibrate.

The target analysis entails the self-consistent fit of the complete PP and PDP data to the same scheme simultaneously. The additional information contained in the PDP experiment is used to extract the spectral and temporal information that cannot be estimated on the basis of the PP data alone: branching ratio, equilibration time constant, “pure” SADS, and ground state relaxation. The time scales and relative yields were varied until the following criteria were fulfilled: (A) the S_1 SADS resembles the PP spectrum measured in hexane, where it is presumed to be the dominant excited state populated, and its lifetime has been fixed to 160 ps, the value measured in hexane (8, 10), because generally the decay of the S_1 state of carotenoids does not depend on the solvent (9); (B) the ICT state SADS is devoid of S_1 contributions and thus contains little of the blue shoulder; (C) the GSI decays to the equilibrated ground state within a picosecond, approximately the lifetime observed in the recovery of the bleach signal after the dump (Figure 2). Finally, the SADS of the GSI has been constrained to have zero amplitude above 575 nm, on the assumption that the GSI must have a spectrum similar to that of the ground state, only slightly red shifted.

The SADS that were estimated by the target analysis fit are shown in Figure 6; the corresponding lifetimes are shown in the compartmental scheme of Figure 5. Within the specific model, the error in the reported values is $<10\%$, and as mentioned earlier, the S_2 SADS is omitted due to distortions by experimental artifacts. The separation of the states has been successful, and the estimated SADS fulfill the set criteria. The unrelaxed ICT state, which is formed from S_2 , decays within 1.1 ps to the equilibrated ICT state; the spectrally selective dump enabled the estimation of the ICT state SADS and its lifetime, which is 8.9 ps. The SADS of the S_1 state peaks around 520 nm and, as in hexane, has an ESA tail to the red. The small scatter of pump light around 530 nm partially contaminates this SADS. The SADS of the GSI contains the ground state bleach up to 510 nm and an induced absorption band which peaks at 545 nm. This GSI subsequently decays to the equilibrated ground state with a 0.9 ps lifetime.

The excited state equilibration between the S_1 and ICT states occurs on a 4.5 ps time scale. This time constant is consistent with the sequential global analysis of the PP data (Figure 2) and results from the combination of the S_1 –ICT coupling rates ($S_1 \rightarrow$ ICT, 12 ps; ICT \rightarrow S_1 , 16 ps, $\pm 20\%$) and the ICT state decay (8.9 ps). Within the applied compartmental model the S_1 –ICT equilibrium is described successfully.

DISCUSSION

The simultaneous target analysis of the PP and PDP data confirmed our hypothesis that the S_1 and the ICT states are distinct entities and has disentangled their spectra and dynamics. According to the modeling, little S_1 ($\sim 5\%$) is produced directly from S_2 after exciting peridinin at 530 nm. Within a few picoseconds after excitation, S_1 gains some population at the expense of the ICT state. The S_1 –ICT state equilibration time (4.5 ps) is faster than the decay of the ICT state (8.9 ps) and considerably faster than the S_1 decay (160 ps); thus, essentially all of the S_1 population decays to the ground state via the ICT state/GSI pathway and not via the direct S_1 – S_0 coupling. This complex dynamics results in the 12.8 ps lifetime found by the fit of the PP data with a sequential model, and the corresponding SADS (Figure 2, solid line) represents the equilibrated populations of the S_1 and the ICT states.

The GSI that we observe cannot be directly observed in PP experiments, because as it decays much faster (0.9 ps) than it is populated (8.9 ps), it does not accumulate appreciable population. Its observation was only possible after the dumping of a significant fraction of ICT population. Although the GSI is a nonequilibrated ground state species, its origin is uncertain; it may arise from vibrational relaxation, structural deformation, solvent dynamics, or some combination thereof. In contrast to vibrational relaxation in the S_1 state of carotenoids (24), clear ground excited state vibrational relaxation dynamics has not been observed thus far in PP measurements of carotenoids (18); time-resolved resonance Raman measurements suggest that it takes several picoseconds (26, 27). Similar GSI’s were observed in PDP experiments on isomerizing chromophores in solution and were ascribed to “twisted” ground state conformers with the resulting subpicosecond relaxations occurring along structural coordinates (19, 20). Additionally, the GSI lifetime is comparable to the time scales found for the excited state solvation dynamics of coumarin in methanol (28). Since the peridinin ICT state is strongly coupled to the polar environment, the nascent ground state population generated by the applied dump pulse undergoes ground state solvation, which has been shown to occur on similar time scales as the excited state analogue (15). Separating these effects is nontrivial. The ICT state is stabilized in polar solvents, suggesting that its formation is stabilized by the generation of a macroscopic polarization by the high dielectric constant environment. This may in turn stabilize a small-scale structural change in peridinin as hypothesized after probing the rise of SE at 950 nm (11). We postulate that the GSI demonstrates a complex relaxation pathway reflecting both ground state solvation dynamics and structural rearrangements.

If we assume that in PCP the 4.5 ps S_1 –ICT equilibration time scale and their connectivity properties are similar to

those observed in methanol, the observation that the S_1 and ICT states have separate populations has significant implications in understanding the function of peridinin. The decay dynamics of the ICT state in PCP matches the rise dynamics of Chl-*a* (6); therefore, since the EET to Chl-*a* is ~ 2.5 ps (5, 6) and faster than the S_1 –ICT equilibration, the ICT state *must* be directly transferring energy to Chl-*a*, without the S_1 state being involved as an intermediate.

Furthermore, the occurrence of a GSI during the relaxation might resolve the apparent energy deficit riddle: how can the ICT state which has emission in the near-IR be an efficient energy donor to the Q_y state of Chl-*a*, which absorbs at 670 nm? The emission spectrum of the ICT state corresponds to the transition to the GSI and not to the equilibrated ground state and, consequently, is not a direct measure of its absolute energy. The four peridinins in the subdomain of the PCP monomer are in close contact with the Chl-*a* molecule; therefore, energy transfer may proceed via a mechanism that depends on the density of acceptor states (29) rather than a classical Förster-type mechanism (30) as previously suggested (6), which requires an appreciable overlap between the emission spectrum of the donor and the absorption spectrum of the acceptor.

CONCLUDING REMARKS

By performing PP and PDP experiments on peridinin in methanol and after target analysis of the measured data, we showed that the ICT state of peridinin, which has also been observed in the other carbonyl-containing carotenoids of marine photosynthetic organisms (31), is a distinct excited state which shares population with the S_1 state on the time scale of a few picoseconds. We also observed an unrelaxed ground state intermediate, which intervenes in the decay of the ICT state and illustrates that, after illumination, peridinin relaxes through a complex pathway. The extrapolation of our observations to the relaxation dynamics of peridinin *in vivo* suggests that the ICT state may be a significant donor of energy to Chl-*a* in PCP.

REFERENCES

- Field, C. B., Behrenfeld, M. J., Randerson, J. T., and Falkowski, P. (1998) Primary production of the biosphere: Integrating terrestrial and oceanic components, *Science* 281, 237–240.
- Falkowski, P. G., and Raven, J. A. (1997) *Aquatic photosynthesis*, Blackwell Science, Oxford.
- Hofmann, E., Wrench, P. M., Sharples, F. P., Hiller, R. G., Welte, W., and Diederichs, K. (1996) Structural basis of light harvesting by carotenoids: Peridinin-chlorophyll-protein from *Amphidinium carterae*, *Science* 272, 1788–1791.
- Bautista, J. A., Hiller, R. G., Sharples, F. P., Gosztola, D., Wasielewski, M., and Frank, H. A. (1999) Singlet and triplet energy transfer in the peridinin-chlorophyll a protein from *Amphidinium carterae*, *J. Phys. Chem. A* 103, 2267–2273.
- Krueger, B. P., Lampoura, S. S., van Stokkum, I. H. M., Papagiannakis, E., Salverda, J. M., Gradinaru, C. C., Rutkauskas, D., Hiller, R. G., and van Grondelle, R. (2001) Energy transfer in the peridinin chlorophyll-a protein of *Amphidinium carterae* studied by polarized transient absorption and target analysis, *Biophys. J.* 80, 2843–2855.
- Zigmantas, D., Hiller, R. G., Sundström, V., and Polivka, T. (2002) Carotenoid to chlorophyll energy transfer in the peridinin-chlorophyll-a-protein complex involves an intramolecular charge transfer state, *Proc. Natl. Acad. Sci. U.S.A.* 99, 16760–16765.
- Polivka, T., and Sundström, V. (2004) Ultrafast dynamics of carotenoid excited states. From solution to natural and artificial systems, *Chem. Rev.* 104, 2021–2071.
- Bautista, J. A., Connors, R. E., Raju, B. B., Hiller, R. G., Sharples, F. P., Gosztola, D., Wasielewski, M. R., and Frank, H. A. (1999) Excited state properties of peridinin: Observation of a solvent dependence of the lowest excited singlet state lifetime and spectral behavior unique among carotenoids, *J. Phys. Chem. B* 103, 8751–8758.
- Frank, H. A., Bautista, J. A., Josue, J., Pendon, Z., Hiller, R. G., Sharples, F. P., Gosztola, D., and Wasielewski, M. R. (2000) Effect of the solvent environment on the spectroscopic properties and dynamics of the lowest excited states of carotenoids, *J. Phys. Chem. B* 104, 4569–4577.
- Zigmantas, D., Polivka, T., Hiller, R. G., Yartsev, A., and Sundström, V. (2001) Spectroscopic and dynamic properties of the peridinin lowest singlet excited states, *J. Phys. Chem. A* 105, 10296–10306.
- Zigmantas, D., Hiller, R. G., Yartsev, A., Sundström, V., and Polivka, T. (2003) Dynamics of excited states of the carotenoid peridinin in polar solvents: Dependence on excitation wavelength, viscosity, and temperature, *J. Phys. Chem. B* 107, 5339–5348.
- Shima, S., Ilagan, R. P., Gillespie, N., Sommer, B. J., Hiller, R. G., Sharples, F. P., Frank, H. A., and Birge, R. R. (2003) Two-photon and fluorescence spectroscopy and the effect of environment on the photochemical properties of peridinin in solution and in the peridinin-chlorophyll-protein from *Amphidinium carterae*, *J. Phys. Chem. A* 107, 8052–8066.
- Vaswani, H. M., Hsu, C. P., Head-Gordon, M., and Fleming, G. R. (2003) Quantum chemical evidence for an intramolecular charge-transfer state in the carotenoid peridinin of peridinin-chlorophyll-protein, *J. Phys. Chem. B* 107, 7940–7946.
- Gai, F., McDonald, J. C., and Anfinrud, P. A. (1997) Pump-dump-probe spectroscopy of bacteriorhodopsin: Evidence for a near-IR excited state absorbance, *J. Am. Chem. Soc.* 119, 6201–6202.
- Changenet-Barret, P., Choma, C., Gooding, E., DeGrado, W., and Hochstrasser, R. M. (2000) Ultrafast dielectric response of proteins from dynamics stokes shifting of coumarin in calmodulin, *J. Phys. Chem. B* 104, 9322.
- Logunov, S. L., Volkov, V. V., Braun, M., and El-Sayed, M. A. (2001) The relaxation dynamics of the excited electronic states of retinal in bacteriorhodopsin by two-pump-probe femtosecond studies, *Proc. Natl. Acad. Sci. U.S.A.* 98, 8475–8479.
- Ruhman, S., Hou, B. X., Friedman, N., Ottolenghi, M., and Sheves, M. (2002) Following evolution of bacteriorhodopsin in its reactive excited state via stimulated emission pumping, *J. Am. Chem. Soc.* 124, 8854–8858.
- Larsen, D. S., Papagiannakis, E., van Stokkum, I. H. M., Vengris, M., Kennis, J. T. M., and van Grondelle, R. (2003) Excited state dynamics of β -carotene explored with dispersed multi-pulse transient absorption, *Chem. Phys. Lett.* 381, 733–742.
- Larsen, D. S., Vengris, M., van Stokkum, I. H. M., van der Horst, M., de Weerd, F. L., Hellingwerf, K. J., and van Grondelle, R. (2004) Photoisomerization and photoionization of the photoactive yellow protein chromophore in solution, *Biophys. J.* 86, 2538–2550.
- Vengris, M., van Stokkum, I. H. M., He, X., Bell, A., Tonge, P., van Grondelle, R., and Larsen, D. S. (2004) Ultrafast excited and ground-state dynamics of the green fluorescent protein chromophore in solution, *J. Phys. Chem. B* 108, 4587–4598.
- Martinson, T. A., and Plumley, F. G. (1995) One-step extraction and concentration of pigments and acyl lipids by sec-butanol from in-vitro and in-vivo samples, *Anal. Biochem.* 228, 123–130.
- Holzwarth, A. R. (1996) in *Biophysical Techniques in Photosynthesis* (Amez, J., and Hoff, A. J., Eds.) pp 75–92, Kluwer, Dordrecht, The Netherlands.
- van Stokkum, I. H. M., Larsen, D. S., and van Grondelle, R. (2004) Global and target analysis of time-resolved spectra, *Biochim. Biophys. Acta* 1657, 82–104.
- de Weerd, F. L., van Stokkum, I. H. M., and van Grondelle, R. (2002) Subpicosecond dynamics in the excited state absorption of all- trans-beta-carotene, *Chem. Phys. Lett.* 354, 38–43.
- Billsten, H. H., Zigmantas, D., Sundström, V., and Polivka, T. (2002) Dynamics of vibrational relaxation in the S_1 state of carotenoids having 11 conjugated C=C bonds, *Chem. Phys. Lett.* 355, 465–470.

26. Yoshizawa, M., Aoki, H., and Hashimoto, H. (2001) Vibrational relaxation of the $2A_g^-$ excited state in all-trans-beta-carotene obtained by femtosecond time-resolved Raman spectroscopy, *Phys. Rev. B* 63.
27. McCamant, D. W., Kim, J. E., and Mathies, R. A. (2002) Vibrational relaxation in beta-carotene probed by picosecond Stokes and anti-Stokes resonance Raman spectroscopy, *J. Phys. Chem. A* 106, 6030–6038.
28. Horng, M. L., Gardecki, J. A., Papazyan, A., and Maroncelli, M. (1995) Subpicosecond measurements of polar solvation dynamics—coumarin-153 revisited, *J. Phys. Chem.* 99, 17311–17337.
29. Dexter, D. L. (1953) A theory of sensitized luminescence in solids, *J. Chem. Phys.* 21, 834–850.
30. Förster, T. (1948) Zwischenmolekulare Energiewanderung und Fluoreszenz, *Ann. Phys.* 2, 55–75.
31. Zigmantas, D., Hiller, R. G., Sharples, F. P., Frank, H. A., Sundstrom, V., and Polivka, T. (2004) Effect of a conjugated carbonyl group on the photophysical properties of carotenoids, *Phys. Chem. Chem. Phys.* 6, 3009–3016.

BI047977R